

1 **Contrasting responses of phytoplankton productivity between coastal and offshore**
2 **surface waters in the Taiwan Strait and the South China Sea to short-term seawater**
3 **acidification**

4

5 Guang Gao¹, Tifeng Wang¹, Jiazhen Sun¹, Xin Zhao¹, Lifang Wang¹, Xianghui Guo¹,
6 Kunshan Gao^{1,2*}

7 ¹State Key Laboratory of Marine Environmental Science & College of Ocean and Earth
8 Sciences, Xiamen University, Xiamen 361005, China

9 ²Co-Innovation Center of Jiangsu Marine Bio-industry Technology, Jiangsu Ocean
10 University, Lianyungang 222005, China

11

12 *Corresponding author: ksgao@xmu.edu.cn

13

14 **Abstract**

15 Seawater acidification (SA) has been documented to either inhibit or enhance or result in
16 no effect on marine primary productivity (PP). In order to examine the effects of SA in
17 changing environments, we investigated the influences of SA (a decrease of 0.4 pH_{total}
18 units with corresponding CO₂ concentrations ranged 22.0–39.7 μM) on PP through
19 deck-incubation experiments at 101 stations in the Taiwan Strait and the South China Sea,
20 including the continental shelf and slope, as well as the deep-water basin. The daily
21 primary productivities in surface seawater under incident solar radiation ranged from 17–
22 306 μg C (μg Chl *a*)⁻¹ d⁻¹, with the responses of PP to SA being region-dependent and the
23 SA-induced changes varying from -88% (inhibition) to 57% (enhancement). The
24 SA-treatment stimulated PP in surface waters of coastal, estuarine and shelf waters, but
25 suppressed it in the South China Sea basin. Such SA-induced changes in PP were
26 significantly related to in situ pH and solar radiation in surface seawater, but negatively
27 related to salinity changes. Our results indicate that phytoplankton cells are more
28 vulnerable to a pH drop in oligotrophic waters. Contrasting responses of phytoplankton
29 productivity in different areas suggest that SA impacts on marine primary productivity
30 are region-dependent and regulated by local environments.

31 **Keywords:** CO₂; Taiwan Strait; seawater acidification; photosynthesis; primary
32 productivity; South China Sea

33 **1 Introduction**

34 The oceans have absorbed about one-third of anthropogenically released CO₂, which
35 increased dissolved CO₂ and decreased pH of seawater (Gattuso et al., 2015), leading to
36 ocean acidification (OA). This process is ongoing and likely intensifying (IPCC, 2019).
37 OA has been shown to result in profound influences on marine ecosystems (see the
38 reviews and literature therein, Mostofa et al., 2016; Doney et al., 2020). Marine
39 photosynthetic organisms, which contribute about half of the global primary production,
40 are also being affected by OA (see the reviews and literatures therein, Riebesell et al.,
41 2018; Gao et al., 2019a). In addition to the slow change of ocean acidification, some
42 processes, such as freshwater inputs, upwelling, typhoons and eddies, can lead to
43 instantaneous CO₂ rising and short-term changes in carbonate chemistry, termed seawater
44 acidification (SA) (Moreau et al., 2017; Yu et al., 2020). Since SA occurs in many
45 locations of the ocean, it is important to understand the responses of the key players of
46 marine biological CO₂ pump, the phytoplankton, to seawater acidification.

47 Elevated CO₂ is well recognized to lessen the dependence of algae and
48 cyanobacteria on energy-consuming CO₂ concentrating mechanisms (CCMs) which
49 concentrate CO₂ around Rubisco, the key site for photosynthetic carbon fixation (Raven
50 & Beardall, 2014 and references therein; Hennon et al., 2015). The energy freed up from
51 the down-regulated CCMs under increased CO₂ concentrations can be applied to other
52 metabolic processes, resulting in a modest increase in algal growth (Wu et al., 2010;
53 Hopkinson et al., 2011; Xu et al., 2017). Accordingly, elevated CO₂ availability could

54 potentially enhance marine primary productivity (Schippers et al., 2004). For instance,
55 across 18 stations in the central Atlantic Ocean primary productivity was stimulated by
56 15–19% under elevated dissolved CO₂ concentrations up to 36 μM (Hein and
57 Sand-Jensen 1997). On the other hand, the neutral effects of seawater acidification (SA)
58 on growth rates of phytoplankton communities were reported in five of six CO₂
59 manipulation experiments in the coastal Pacific (Tortell et al., 2000). Furthermore,
60 simulated future SA reduced surface PP in pelagic surface waters of Northern South
61 China Sea and East China Sea (Gao et al., 2012). It seems that the impacts of SA on PP
62 could be region-dependent. The varying effects of SA may be related to the regulation of
63 other factors such as light intensity (Gao et al., 2012), temperature (Holding et al., 2015),
64 nutrients (Tremblay et al., 2006) and community structure (Dutkiewicz et al., 2015).

65 Taiwan Strait of the East China Sea, located between southeast Mainland China and
66 the Island of Taiwan, is an important channel in transporting water and biogenic elements
67 between the East China Sea and the South China Sea. Among the Chinese coastal areas,
68 the Taiwan Strait is distinguished by its unique location. In addition to riverine inputs, it
69 also receives nutrients from upwelling (Hong et al., 2011). Primary productivity is much
70 higher in coastal waters than that in basin zones due to an increased supply of nutrients
71 through river runoff and upwelling (Chen, 2003; Cloern et al., 2014). The South China
72 Sea, located from the equator to 23.8 °N, from 99.1 to 121.1 °E and encompassing an area
73 of about 3.5×10^6 km², is one of the largest marginal seas in the world. As a marginal sea

74 of the Western Pacific Ocean, it has a deep semi-closed basin (with depths > 5000 m) and
75 wide continental shelves, characterized by a tropical and subtropical climate (Jin et al.,
76 2016). Approximately 80% of ocean organic carbon is buried in the Earth's continental
77 shelves and therefore continental margins play an essential role in the ocean carbon cycle
78 (Hedges & Keil, 1995). Investigating how SA affects primary productivity in the Taiwan
79 Strait and the South China Sea could help us to understand the contribution of marginal
80 seas to carbon sink under the future CO₂-increased scenarios. Although small-scale
81 studies on SA impacts have been conducted in the East China Sea and the South China
82 Sea (Gao et al., 2012, 2017), our understanding of how SA affects PP in marginal seas is
83 still fragmentary and superficial. In this study, we conducted three cruises in the Taiwan
84 Strait and the South China Sea, covering an area of 8.3×10^5 km², and aimed to provide
85 in-depth insight into how SA and/or episodic pCO₂ rise affects PP in marginal seas with
86 comparisons to other types of waters.

87 **2 Materials and Methods**

88 **2.1 Investigation areas**

89 To study the impacts of projected SA (dropping by ~0.4 pH) by the end of this
90 century (RCP8.5) on marine primary productivity in different areas (Gattuso et al., 2015),
91 we carried out deck-based experiments during the 3 cruises supported by National
92 Natural Science Foundation of China (NSFC), which took place in the Taiwan Strait (Jul
93 14th–25th, 2016), the South China Sea basin (Sep 6–24th, 2016), and the West South China

94 Sea (Sep 14th to Oct 24th, 2017), respectively. The experiments were conducted at 101
95 stations with coverage of 12 °N–26 °N and 110 °E–120 °E (Fig. 1). Investigation areas
96 include the continental shelf (0–200 m, 22 stations) and the slope (200–3400 m, 44
97 stations), and the vast deep-water basin (> 3400 m, 35 stations). In the continental shelf,
98 the areas with depth < 50 m are defined as coastal zones (9 stations).

99 **2.2 Measurements of temperature and carbonate chemistry parameters**

100 The temperature and salinity of surface seawater at each station were monitored with
101 an onboard CTD (Seabird, USA). pH_{NBS} was measured with an Orion 2-Star pH meter
102 (Thermo scientific, USA) that was calibrated with standard National Bureau of Standards
103 (NBS) buffers ($\text{pH}=4.01, 7.00, \text{ and } 10.01$ at $25.0\text{ }^{\circ}\text{C}$; Thermo Fisher Scientific Inc., USA).
104 After the calibration, the electrode of pH meter was kept in surface seawater for half an
105 hour and then the formal measurements were conducted. The analytical precision was
106 ± 0.001 . Total alkalinity (TA) was determined using Gran titration on a 25-mL sample
107 with a TA analyzer (AS-ALK1, Apollo SciTech, USA) that was regularly calibrated with
108 certified reference materials supplied by A. G. Dickson at the Scripps Institution of
109 Oceanography (Gao et al., 2018a). The analytical precision was $\pm 2\ \mu\text{mol kg}^{-1}$. CO_2
110 concentration in seawater and the pH_{Total} (pH_{T}) values were calculated by using CO2SYS
111 (Pierrot et al., 2006) with the input of pH_{NBS} and TA data.

112 **2.3 Solar radiation**

113 The incident solar radiation intensity during the cruises was recorded with an

114 Eldonet broadband filter radiometer (Eldonet XP, Real Time Computer, Germany). This
115 device has three channels for PAR (400–700 nm), UV-A (315–400 nm) and UV-B (280–
116 315 nm) irradiance, respectively, which records the means of solar radiations over each
117 minute. The instrument was fixed at the top layer of the ship to avoid shading.

118 **2.4 Determination of primary productivity**

119 Surface seawater (0–1m) was collected with a 10 L acid-cleaned (1 M HCl) plastic
120 bucket and pre-filtered (200 μm mesh size) to remove large grazers. To prepare high CO_2
121 (HC) seawater, CO_2 -saturated seawater was added into pre-filtered seawater until a
122 decrease of ~ 0.4 units in pH (corresponding CO_2 concentrations being 22.0–39.7 μM)
123 was approached (Gattuso et al., 2010). Seawater that was collected from the same
124 location as PP and filtered by cellulose acetate membrane (0.22 μm) was used to make
125 the CO_2 -saturated seawater, which was made by directly flushing with pure CO_2 until pH
126 reached values around 4.50. When saturated- CO_2 seawater was added to the HC
127 treatment, equivalent filtered seawater (without flushing with CO_2) was also added to the
128 ambient CO_2 (AC) treatment as a control. The ratios of added saturated- CO_2 seawater to
129 incubation seawater were about 1:1000. Samples were incubated within half an hour after
130 they were collected. Prepared AC and HC seawater was allocated into 50-mL quartz
131 tubes in triplicate, inoculated with 5 μCi (0.185 MBq) $\text{NaH}^{14}\text{CO}_3$ (ICN Radiochemicals,
132 USA), and then incubated for 24 h (over a day-night cycle) under 100 % incident solar
133 irradiances in a water bath for temperature control by running through surface seawater.

134 Due to heating by the deck, the temperatures in the water bath were 0–2 °C higher than in
135 situ surface seawater temperatures. TA and pH of seawater before and after 24h
136 incubation were measured to monitor the changes in carbonate systems. After the
137 incubation, the cells were filtered onto GF/F filters (Whatman) and immediately frozen at
138 –20 °C for later analysis. In the laboratory, the frozen filters were transferred to 20 mL
139 scintillation vials, thawed and exposed to HCl fumes for 12 h, and dried (55 °C, 6 h) to
140 expel non-fixed ¹⁴C, as previously reported (Gao et al., 2017). Then 3 mL scintillation
141 cocktail (Perkin Elmer®, OptiPhase HiSafe) was added to each vial. After 2 h of reaction,
142 the incorporated radioactivity was counted by a liquid scintillation counting (LS 6500,
143 Beckman Coulter, USA). The carbon fixation for 24 h incubation was taken as
144 chlorophyll (Chl) *a*-normalized daily primary productivity (PP, µg C (µg Chl *a*)⁻¹) (Gao et
145 al., 2017). The changes (%) of PP induced by SA were expressed as $(PP_{HC} -$
146 $PP_{AC})/PP_{AC} \times 100$, where PP_{HC} and PP_{AC} are the daily primary productivity under HC and
147 AC, respectively.

148 **2.5 Chl *a* measurement**

149 Pre-filtered (200 µm mesh size) surface seawater (500–2000 mL) at each station was
150 filtered onto GF/F filter (25 mm, Whatman) and then stored at -80 °C. After returning to
151 laboratory, phytoplankton cells on the GF/F filter were extracted overnight in absolute
152 methanol at 4 °C in darkness. After centrifugation (5000 g for 10 min), the absorption
153 values of the supernatants were analyzed by a UV–VIS spectrophotometer (DU800,

154 Beckman, Fullerton, California, USA). The concentration of chlorophyll *a* (Chl *a*) was
155 calculated according to Porra (2002).

156 **2.6 Data analysis**

157 The data of environmental parameters were expressed in raw and the data of PP were
158 the means of triplicate incubations. Two-way analysis of variance (ANOVA) was used to
159 analyze the effects of SA and location on PP. Least significant difference (LSD) was used
160 to for *post hoc* analysis. Linear fitting analysis was conducted with Pearson correlation
161 analysis to assess the relationship between PP and environmental factors. A 95%
162 confidence level was used in all analyses.

163 **3 Results**

164 During the cruises, surface temperature ranged from 25.0 to 29.9 °C in the Taiwan
165 Strait and from 27.1 to 30.2 °C in the South China Sea (Fig. 2a). Surface salinity ranged
166 from 30.0 to 34.0 in the Taiwan Strait and from 31.0 to 34.3 in the South China Sea (Fig.
167 2b). The lower salinities were found in the estuaries of Minjiang and Jiulong Rivers as
168 well as Mekong River-induced Rip current. High salinities were found in the South China
169 Sea basin. Surface pH_T changed between 7.99–8.20 in the Taiwan Strait with the higher
170 values in the estuary of Minjiang River (Fig. 2c). Compared to the Taiwan Strait, the
171 South China Sea had lower surface pH (7.91–8.08) with the lowest value near the island
172 in the Philippines. TA ranged from 2100 to 2359 $\mu\text{mol kg}^{-1}$ SW in the Taiwan Strait and
173 2126 to 2369 $\mu\text{mol kg}^{-1}$ SW in the South China Sea (Fig. 2d). The lowest value occurred

174 in the estuary of Minjiang River. CO₂ concentration in surface seawater changed from
175 6.4–13.3 μmol kg⁻¹ SW in the Taiwan Strait, and 9.3–14.3 μmol kg⁻¹ SW in the South
176 China Sea (Fig. 2e). It showed an opposite pattern to surface pH, with the lowest value in
177 the estuary of Minjiang River in the Taiwan Strait and the highest value in the South
178 China Sea near the islands in the Philippines. During the PP investigation period, the
179 daytime mean PAR intensity ranged from 126.6 to 145.2 W m⁻² in the Taiwan Strait and
180 37.3 to 150.0 W m⁻² in the South China Sea (Fig. 2f).

181 The concentration of Chl *a* ranged from 0.11 to 12.13 μg L⁻¹ in the Taiwan Strait (Fig.
182 3). The highest concentration occurred in the estuary of the Minjiang River. The
183 concentration of Chl *a* in the South China Sea ranged from 0.037 to 7.43 μg L⁻¹. The
184 highest concentration was found in the coastal areas of Guangdong province in China.
185 For both the Taiwan Strait and the South China Sea, there were high Chl *a* concentrations
186 (> 1.0 μg L⁻¹) in coastal areas, particularly in the estuaries of the Minjing River, Jiulong
187 River and Pearl River. On the contrary, Chl *a* concentrations in offshore areas were lower
188 than 0.2 μg L⁻¹.

189 Surface primary productivity changed from 99 to 302 μg C (μg Chl *a*)⁻¹ d⁻¹ in the
190 Taiwan Strait, and from 17 to 306 μg C (μg Chl *a*)⁻¹ d⁻¹ in the South China Sea (Fig. 4).
191 High surface primary productivity (> 200 μg C (μg Chl *a*)⁻¹ d⁻¹) was found in the
192 estuaries of the Minjing River, Jiulong River, and Pearl River and areas near the East of
193 Vietnam. In basin zones, the surface primary productivity was usually lower than 100 μg

194 C ($\mu\text{g Chl } a$)⁻¹ d⁻¹.

195 A series of onboard CO₂-enrich experiments in the investigated regions were
196 conducted during three cruises. In HC treatments, pH_{total} decreased by 0.34–0.43 units,
197 while pCO₂ and CO₂ increased by 676–982 μatm and 17–25 $\mu\text{mol kg}^{-1}$ SW, respectively
198 (Table S1). Carbonate chemistry parameters after 24 h of incubation were stable ($\Delta\text{pH} <$
199 0.06 , $\Delta\text{TA} < 53 \mu\text{mol kg}^{-1}$ SW), indicating the successful manipulation (Table S1). It
200 was observed that instantaneous effects of elevated pCO₂ on primary productivity of
201 surface phytoplankton community in all investigated regions ranged from -88%
202 (inhibition) to 57% (promotion), revealing significant regional differences among
203 continental shelf, slope and deep-water basin (ANOVA, $F_{(2, 98)} = 3.747$, $p = 0.027$, Fig. 5).
204 Among 101 stations, 70 stations showed insignificant SA effects. SA increased PP at 6
205 stations and reduced PP at 25 stations. Positive effects of SA on surface primary
206 productivity were observed in the Taiwan Strait and the western South China Sea (Fig. 5,
207 red-yellow shading areas), with the maximal enhancement of 57% in the station
208 approaching the Mekong River plume (LSD, $p < 0.001$). Reductions in PP induced by the
209 elevated CO₂ were mainly found in the central South China Sea basin within the latitudes
210 of 10 °N to 14 °N and the longitudes of 114.5 °E to 118 °E (Fig. 5, blue-purple shading
211 areas), with inhibition rates ranging from 24% to 88% (Fig. 5, LSD, $p < 0.05$). These
212 results showed a region-related effect of SA on photosynthetic carbon fixation of surface
213 phytoplankton assemblages. Overall, the elevated pCO₂ had neutral or positive effects on

214 primary productivity in the continental shelf and slope regions, while having adverse
215 effects in the deep-water basin.

216 By analyzing the correlations between SA-induced PP changes and regional
217 environmental parameters (Table S2), we found that SA-induced changes in
218 phytoplankton primary productivity was significantly positively related with *in situ* pH (p
219 < 0.001 , $r = 0.379$), and PAR density ($p = 0.002$, $r = 0.311$) (Fig. 6). On the other hand,
220 the influence induced by SA was negatively related to salinity that ranged from 30.00 to
221 34.28 ($p < 0.001$, $r = -0.418$).

222 **4 Discussion**

223 In the present study, we found that the elevated pCO₂ and associated pH drop
224 increased or did not affect PP in the continental shelf and slope waters but reduced it in
225 basin waters. Our results suggested that the enhanced effects of the SA treatment on
226 photosynthetic carbon fixation depend on regions of different physicochemical conditions,
227 including pH, light intensity and salinity. In addition, coastal diatoms appear to benefit
228 more from SA than pelagic ones (Li et al., 2016). Therefore, community structure
229 differences might also be responsible for the contrasts of the short-term high
230 CO₂-induced acidification between coastal and basin waters.

231 SA is deemed to have two kinds of effects at least (Xu et al., 2017; Shi et al., 2019).
232 The first one is the enrichment of CO₂, which is usually beneficial for photosynthetic
233 carbon fixation and growth of algae because insufficient ambient CO₂ limits algal

234 photosynthesis (Hein & Sand-Jensen, 1997; Bach & Taucher, 2019). The other effect is
235 the decreased pH which could be harmful because it disturbs the acid-base balance
236 between extracellular and intracellular environments. For instance, the decreased pH
237 projected for future SA was shown to reduce the growth of the diazotroph *Trichodesmium*
238 (Hong et al., 2017), decrease PSII activity by reducing the removal rate of PsbD (D2)
239 (Gao et al., 2018b) and increase mitochondrial and photo-respirations in diatoms and
240 phytoplankton assemblages (Yang and Gao 2012, Jin et al., 2015). In addition, SA could
241 reduce the Rubisco transcription of diatoms, which also contributed to the decreased
242 growth (Endo et al., 2015). Therefore, the net impact of SA depends on the balance
243 between its positive and negative effects, leading to enhanced, inhibited or neutral
244 influences, as reported in diatoms (Gao et al., 2012, Li et al., 2021) and phytoplankton
245 assemblages in the Arctic and subarctic shelf seas (Hoppe et al., 2018), the North Sea
246 (Eberlein et al., 2017) and the South China Sea (Wu and Gao 2010, Gao et al., 2012). The
247 balance of positive and negative effects of SA can be regulated by other factors, including
248 pH, light intensity, salinity, population structure, etc. (Gao et al., 2019a, b; Xie et al.,
249 2022).

250 In the present study, SA increased or did not affect PP in coastal waters but reduced it
251 in offshore waters, which is significantly related to pH, light intensity and salinity (Fig. 6).
252 The effect of SA changed from negative to positive with the increase of local pH. The
253 higher pH occurred in coastal zones which may be caused by higher biomass of

254 phytoplankton (Fig. 3). Higher pH caused by intensive photosynthesis of phytoplankton
255 is accompanied with decreased CO₂ levels. In this case, CO₂ is more limiting for
256 photosynthesis of phytoplankton compared to lower pH. Therefore, SA could stimulate
257 primary productivity via supplying more available CO₂ (Hurd et al., 2019). On the other
258 hand, lower pH occurred in the deep-water basin. Lower pH represents higher CO₂
259 availability. CO₂ is not limited or less limited in this case. Therefore, more CO₂ brought
260 by SA may not benefit the photosynthesis of phytoplankton. Instead, decreased pH
261 accompanied by SA may inhibit photosynthesis or growth of phytoplankton, which is
262 found in cyanobacteria (Hong et al., 2017). Furthermore, the negative effects of SA are
263 particularly significant when nutrient is limited (Li et al., 2018). The nutrient levels in the
264 basin are usually lower than on the shelf (Yuan et al., 2011; Lu et al., 2020; Du et al.,
265 2021), which may exacerbate the negative effects of SA in the basin zone.

266 The negative effects of SA disappeared with increasing light intensity in this study.
267 This results in inconsistent with the study of Gao et al (2012), in which SA increased
268 photosynthetic carbon fixation of three diatoms (*Phaeodactylum tricornutum*,
269 *Thalassiosira pseudonana* and *Skeletonema costatum*) under lower light intensities but
270 decreased it under higher light intensities. The divergent findings may be due to different
271 population structure that varies in different areas. Coastal zones where nutrients are
272 relatively sufficient usually have abundant diatoms while picophytoplankton mainly
273 *Prochlorococcus* and *Synechococcus*, dominate oligotrophic areas (Xiao et al., 2018,

274 Zhong et al., 2020). In this study, most investigated areas are oligotrophic and thus the
275 response of local phytoplankton to the combination of light intensity and SA may be
276 different from diatoms. Meanwhile, the weak correlation ($r = 0.311$) between light
277 intensity and SA effect suggests the deviation from the linear relationship in the context
278 of multiple variables needs to be further illuminated in future studies. It is worth noting
279 that the samples were not mixed down in the water bath in the present study and exposed
280 to 100% incident solar irradiances. Lower incident solar irradiances or some devices can
281 be used to simulate seawater mixing in future studies. A negative correlation between
282 SA-induced changes in PP and salinity was found in this study. The decrease in salinity
283 (from 35 to 30) has been shown to alleviate the negative effect of SA on the
284 photosynthetic carbon fixation of the coccolithorporid *Emiliana huxleyi* (Xu et al., 2020)
285 although the potential mechanisms remain unknown. On the other hand, the change of
286 salinity (from 6 to 3) did not affect the effective quantum yield of microplanktonic
287 community in the Baltic Sea grown under different CO₂ levels (Wulff et al., 2018). In this
288 study, the negative relationship between salinity and SA effects seems to be an
289 autocorrelation between salinity and in situ pH (Fig. S1) because lower salinity occurred
290 in coastal waters where seawater pH was higher while the basin zone usually had higher
291 salinities and lower pH.

292 The specific environmental conditions have profound effects on shaping diverse
293 dominant phytoplankton groups (Boyd et al., 2010). Larger eukaryotic groups (especially

294 diatoms) usually dominate the complex coastal regions, while picophytoplankton
295 (*Prochlorococcus* and *Synechococcus*), characterizing with more efficient nutrient uptake,
296 dominate the relatively stable offshore waters (Dutkiewicz et al., 2015). In summer and
297 early autumn, previous investigations demonstrated that diatoms dominated in the
298 northern waters and the Taiwan Strait (coastal and shelf regions) with high abundances of
299 phytoplankton, which is consistent with our Chl *a* data; *Prochlorococcus* and
300 *Synechococcus* dominated in the South China Sea basin and the north of South China Sea
301 (slope and basin regions) (Xiao et al., 2018, Zhong et al., 2020). In addition, it has been
302 reported that larger cells benefit more from SA because a thicker diffusion layer around
303 the cells limits the transport of CO₂ (Feng et al., 2010; Wu et al., 2014). In contrast, a
304 thinner diffusion layer and higher surface to volume ratio in smaller phytoplankton cells
305 can make them easier to transport CO₂ near the cell surface and within the cells, and
306 therefore picophytoplankton species are less CO₂-limited (Bao and Gao, 2021). Therefore,
307 different community structures between coastal and basin areas could also be responsible
308 for the enhanced and inhibitory effects of SA. It is worth noting that seasonality may also
309 lead to the differential effects of SA on primary productivity since the Taiwan Strait
310 cruise was conducted in July and the cruises of the South China Sea basin and the West
311 South China Sea were conducted in September. The SST and solar PAR intensity of the
312 Taiwan Strait in July was 2–3 °C and $22 \pm 22 \text{ W m}^{-2}$ higher than that in September (Zhang
313 et al., 2008, 2009; Table S3). Although the effects of SA were not related to temperature

314 as shown in this study (Table S2), the higher solar radiation in July may contribute to the
315 positive effect of SA on primary productivity. In addition, seasonal phytoplankton species
316 succession may also affect the response to SA (Xiao et al., 2018).

317 **5 Conclusions**

318 By investigating the impacts of the elevated pCO₂ on PP in the Taiwan Strait and the
319 South China Sea, we demonstrated that such short SA-treatments induced changes in PP
320 were mainly related to pH, light intensity and salinity based on Pearson correlation
321 coefficients, supporting the hypothesis that negative impacts of SA on PP increase from
322 coastal to basin waters (Gao et al., 2019a). In addition, changes in phytoplankton
323 community structure may also modulate the SA induced variability. In view of ocean
324 climate changes, strengthened stratification due to global warming would reduce the
325 upward transport of nutrients and thus marine primary productivity. The negative effect
326 of SA in basin zones may further reduce primary productivity. Meanwhile, PP in some
327 coastal waters may be increased by SA.

328 *Data availability.* All data are included in the article or Supplement.

329 *Author contributions.* KG and TW developed the original idea and designed the research.
330 TW and JS carried out fieldwork. TW and XZ did the laboratory analyses. GG provided
331 statistical analyses and prepared figures. GG, KG, and XZ wrote the manuscript. All
332 contributed to revising the paper.

333 *Competing interests.* The contact author has declared that neither they nor their

334 co-authors have any competing interests.

335 *Disclaimer.* Publisher's note: Copernicus Publications remains neutral with regard to
336 jurisdictional claims in published maps and institutional affiliations.

337 *Acknowledgements.* This work was supported by the National Natural Science
338 Foundation of China (41720104005, 41890803, 41721005, and 42076154) and the
339 Fundamental Research Funds for the Central Universities (20720200111). The authors
340 are grateful to the students He Li, Xiaowen Jiang and Shanying Tong, and the laboratory
341 technicians Wenyan Zhao and Xianglan Zeng. We appreciate the NFSC Shiptime Sharing
342 Project (project number: 41849901) for supporting the Taiwan Strait cruise
343 (NORC2016-04). We appreciate the chief scientists Yihua Cai, Huabin Mao and Chen Shi
344 and the R/V Yanping II, Shiyan I and Shiyan III for leading and conducting the cruises.

345 **References**

346 Bach, L. T., and Taucher, J.: CO₂ effects on diatoms: a synthesis of more than a decade of
347 ocean acidification experiments with natural communities, *Ocean Sci.*, 15,
348 1159-1175, 2019.

349 Bao, N., and Gao, K.: Interactive effects of elevated CO₂ concentration and light on the
350 picophytoplankton *Synechococcus*, *Front. Mar. Sci.*, 8, 1-7, 2021.

351 Boyd, P. W., Strzepek, R., Fu, F. X., and Hutchins, D. A.: Environmental control of open-
352 ocean phytoplankton groups: Now and in the future, *Limnol. Oceanogr.*, 55,
353 1353-1376, 2010.

354 Chen, C. T. A.: Rare northward flow in the Taiwan Strait in winter: A note, *Cont. Shelf*
355 *Res.*, 23, 387-391, 2003.

356 Cloern, J. E., Foster, S.Q. and Kleckner, A. E.: Phytoplankton primary production in the
357 world's estuarine-coastal ecosystems, *Biogeosciences*, 11, 2477-2501, 2014.

358 Doney, S. C., Busch, D. S., Cooley, S. R., and Kroeker, K. J.: The impacts of ocean
359 acidification on marine ecosystems and reliant human communities, *Annu. Rev. Env.*
360 *Resour.*, 45, 83-112, 2020.

361 Du, C., He, R., Liu, Z., Huang, T., Wang, L., Yuan, Z., Xu, Y., Wang, Z. and Dai, M.:
362 Climatology of nutrient distributions in the South China Sea based on a large data
363 set derived from a new algorithm. *Prog. Oceanogr.*, 195, 102586, 2021.

364 Dutkiewicz, S., Morris, J. J., Follows, M. J., Scott, J., Levitan, O., Dyhrman, S. T., and
365 Berman-Frank, I.: Impact of ocean acidification on the structure of future
366 phytoplankton communities, *Nat. Clim. Change*, 5, 1002-1006, 2015.

367 Eberlein, T., Wohlrab, S., Rost, B., John, U., Bach, L. T., Riebesell, U., and Van de Waal,
368 D. B.: Effects of ocean acidification on primary production in a coastal North Sea
369 phytoplankton community, *Plos One*, 12, 1-15, 2017.

370 Endo, H., Sugie, K., Yoshimura, T., and Suzuki, K.: Effects of CO₂ and iron availability
371 on *rbcL* gene expression in Bering Sea diatoms, *Biogeosciences*, 12, 2247-2259,
372 2015.

373 Feng, Y., Hare, C. E., Rose, J. M., Handy, S. M., DiTullio, G. R., Lee, P. A., Smith, W. O.,

374 Pelouin, J., Tozzi, S., Sun, J., Zhang, Y., Dunbar, R. B., Long, M. C., Sohst, B.,
375 Lohan, M., and Hutchins, D. A.: Interactive effects of iron, irradiance and CO₂ on
376 Ross Sea phytoplankton, *Deep-Sea Res. PT. I*, 57, 368-383, 2010.

377 Gao, G., Xu, Z. G., Shi, Q., and Wu, H. Y.: Increased CO₂ exacerbates the stress of
378 ultraviolet radiation on photosystem II function in the diatom *Thalassiosira*
379 *weissflogii*, *Environ. Exp. Bot.*, 156, 96-105, 2018b.

380 Gao, G., Jin, P., Liu, N., Li, F. T., Tong, S. Y., Hutchins, D. A., and Gao, K. S.: The
381 acclimation process of phytoplankton biomass, carbon fixation and respiration to the
382 combined effects of elevated temperature and pCO₂ in the northern South China Sea,
383 *Mar. Pollut. Bull.*, 118, 213-220, 2017.

384 Gao, G., Qu, L., Xu, T., Burgess, J.G., Li, X. and Xu, J.: Future CO₂-induced ocean
385 acidification enhances resilience of a green tide alga to low-salinity stress. *ICES J.*
386 *Mar. Sci.*, 76, 2437-2445, 2019b.

387 Gao, G., Xia, J. R., Yu, J. L., Fan, J. L., and Zeng, X. P.: Regulation of inorganic carbon
388 acquisition in a red tide alga (*Skeletonema costatum*): The importance of phosphorus
389 availability, *Biogeosciences*, 15, 4871-4882, 2018a.

390 Gao, K. S., Beardall, J., Häder, D. P., Hall-Spencer, J. M., Gao, G., and Hutchins, D. A.:
391 Effects of ocean acidification on marine photosynthetic organisms under the
392 concurrent influences of warming, UV radiation, and deoxygenation, *Front. Mar.*
393 *Sci.*, 6, 1-18, 2019a.

394 Gao, K. S., Xu, J. T., Gao, G., Li, Y. H., Hutchins, D. A., Huang, B. Q., Wang, L., Zheng,
395 Y., Jin, P., Cai, X. N., Hader, D. P., Li, W., Xu, K., Liu, N. N., and Riebesell, U.:
396 Rising CO₂ and increased light exposure synergistically reduce marine primary
397 productivity, *Nat. Clim. Change*, 2, 519-523, 2012.

398 Gattuso, J. P., Gao, K. S., Lee, K., Rost, B., and Schulz, K. G.: Approaches and tools to
399 manipulate the carbonate chemistry, pp 41-52. Guide to best practices for ocean
400 acidification research and data reporting, edited by: Riebesell, U., Fabry, V. J.,
401 Hansson, L., and Gattuso J.-P., Luxembourg: Publications Office of the European
402 Union, 2010.

403 Gattuso, J. P., Magnan, A., Bill é R., Cheung, W. W. L., Howes, E. L., Joos, F., Allemand,
404 D., Bopp, L., Cooley, S. R., Eakin, C. M., Hoegh-Guldberg, O., Kelly, R. P., Portner,
405 H. O., Rogers, A. D., Baxter, J. M., Laffoley, D., Osborn, D., Rankovic, A., Rochette,
406 J., Sumaila, U. R., Treyer, S., and Turley, C.: Contrasting futures for ocean and
407 society from different anthropogenic CO₂ emissions scenarios, *Science*, 349,
408 aac4722, 2015.

409 Hedges, J. I., and Keil, R. G.: Sedimentary organic matter preservation: an assessment
410 and speculative synthesis, *Mar. Chem.*, 49, 81-115, 1995.

411 Hein, M., and Sand-Jensen, K.: CO₂ increases oceanic primary production, *Nature*, 388,
412 526-527, 1997.

413 Hennon, G. M. M., Ashworth, J., Groussman, R. D., Berthiaume, C., Morales, R. L.,

414 Baliga, N. S., Orellana, M. V., and Armbrust, E. V.: Diatom acclimation to elevated
415 CO₂ via cAMP signalling and coordinated gene expression, *Nat. Clim. Change*, 5,
416 761-765, 2015.

417 Holding, J. M., Duarte, C. M., Sanz-Martín, M., Mesa, E., Arrieta, J. M., Chierici, M.,
418 Hendriks, I. E., Garcia-Corral, L. S., Regaudie-de-Gioux, A., Delgado, A., Reigstad,
419 M., Wassmann, P., and Agusti, S.: Temperature dependence of CO₂-enhanced
420 primary production in the European Arctic Ocean, *Nat. Clim. Change*, 5, 1079-1082,
421 2015.

422 Hong, H. S., Chai, F., Zhang, C. Y., Huang, B. Q., Jiang, Y. W., and Hu, J. Y.: An
423 overview of physical and biogeochemical processes and ecosystem dynamics in the
424 Taiwan Strait, *Cont. Shelf Res.*, 31, S3-S12, 2011.

425 Hong, H. Z., Shen, R., Zhang, F. T., Wen, Z. Z., Chang, S. W., Lin, W. F., Kranz, S. A.,
426 Luo, Y. W., Kao, S. J., Morel, F. M. M. and Shi, D. L.: The complex effects of ocean
427 acidification on the prominent N₂-fixing cyanobacterium *Trichodesmium*. *Science*,
428 356, 527-530, 2017.

429 Hopkinson, B. M., Dupont, C. L., Allen, A. E., and Morel, F. M.: Efficiency of the
430 CO₂-concentrating mechanism of diatoms, *P. Natl. Acad. Sci. USA.*, 108, 3830-3837,
431 2011.

432 Hoppe, C. J. M., Wolf, K. K. E., Schuback, N., Tortell, P. D., and Rost, B.: Compensation
433 of ocean acidification effects in Arctic phytoplankton assemblages. *Nat. Clim.*

434 Change, 8, 529-533, 2018.

435 Hurd, C.L., Beardall, J., Comeau, S., Cornwall, C.E., Havenhand, J.N., Munday, P.L.,
436 Parker, L.M., Raven, J.A. and McGraw, C.M.: Ocean acidification as a multiple
437 driver: how interactions between changing seawater carbonate parameters affect
438 marine life. *Mari. Freshwater Res.*, 71, 263-274, 2019.

439 IPCC, 2019: IPCC Special Report on the Ocean and Cryosphere in a Changing Climate
440 [H.-O. Pörtner, D.C. Roberts, V. Masson-Delmotte, P. Zhai, M. Tignor, E.
441 Poloczanska, K. Mintenbeck, A. Alegría, M. Nicolai, A. Okem, J. Petzold, B. Rama,
442 N.M. Weyer (eds.)]. In press.

443 Jin, P., Gao, G., Liu, X., Li, F. T., Tong, S. Y., Ding, J. C., Zhong, Z. H., Liu, N. N., and
444 Gao, K. S.: Contrasting photophysiological characteristics of phytoplankton
445 assemblages in the Northern South China Sea, *Plos One*, 11, 1-16, 2016.

446 Jin, P., Wang, T. F., Liu, N. N., Dupont, S., Beardall, J., Boyd, P. W., Riebesell, U., and
447 Gao, K. S.: Ocean acidification increases the accumulation of toxic phenolic
448 compounds across trophic levels, *Nat. Commun.*, 6, 1-6, 2015.

449 Li, F. T., Wu, Y. P., Hutchins, D. A., Fu, F. X., and Gao, K. S.: Physiological responses of
450 coastal and oceanic diatoms to diurnal fluctuations in seawater carbonate chemistry
451 under two CO₂ concentrations, *Biogeosciences*, 13, 6247-6259, 2016.

452 Li, F. T., Beardall, J., and Gao, K. S.: Diatom performance in a future ocean: interactions
453 between nitrogen limitation, temperature, and CO₂-induced seawater acidification,

454 ICES J. Mar. Sci., 75, 1451-1464, 2018.

455 Li, H. X., Xu, T. P., Ma, J., Li, F. T., and Xu, J. T.: Physiological responses of
456 *Skeletonema costatum* to the interactions of seawater acidification and the
457 combination of photoperiod and temperature, Biogeosciences, 18, 1439-1449, 2021.

458 Lu, Z., Gan, J., Dai, M., Zhao, X. and Hui, C. R.: Nutrient transport and dynamics in the
459 South China Sea: A modeling study. Prog. Oceanogr., 183, 102308, 2020.

460 Moreau, S., Penna, A. D., Llorc, J., Patel, R., Langlais, C., Boyd, P. W., Matear, R. J.,
461 Phillips, H. E., Trull, T. W., Tilbrook, B. and Lenton, A.: Eddy-induced carbon
462 transport across the Antarctic Circumpolar Current. Global Biogeochem. Cy., 31,
463 1368-1386, 2017

464 Mostofa, K.M., Liu, C.Q., Zhai, W., Minella, M., Vione, D., Gao, K., Minakata, D.,
465 Arakaki, T., Yoshioka, T., Hayakawa, K. and Konohira, E.: Reviews and Syntheses:
466 Ocean acidification and its potential impacts on marine ecosystems, Biogeosciences,
467 13, 1767-1786, 2016.

468 Pierrot, D., Wallace, D.W. R., and Lewis, E.: MS Excel program developed for CO₂
469 system calculations. ORNL/CDIAC-105a, Carbon Dioxide Information Analysis
470 Center, Oak Ridge National Laboratory, US Department of Energy, Oak Ridge,
471 Tennessee, USA., 2006.

472 Porra, R. J.: The chequered history of the development and use of simultaneous equations
473 for the accurate determination of chlorophylls a and b, Photosynth. Res., 73,

474 149-156, 2002.

475 Raven, J. A., and Beardall, J.: CO₂ concentrating mechanisms and environmental change,
476 *Aquat. Bot.*, 118, 24-37, 2014.

477 Schippers, P., Lüring, M., and Scheffer, M.: Increase of atmospheric CO₂ promotes
478 phytoplankton productivity, *Ecol. Lett.*, 7, 446-451, 2004.

479 Shi, D. L., Hong, H. Z., Su, X., Liao, L. R., Chang, S. W., and Lin, W. F.: The
480 physiological response of marine diatoms to ocean acidification: Differential roles of
481 seawater pCO₂ and pH, *J. Phycol.*, 55, 521-533, 2019.

482 Tortell, P. D., Rau, G. H., and Morel, F. M. M.: Inorganic carbon acquisition in coastal
483 Pacific phytoplankton communities, *Limnol. Oceanogr.*, 45, 1485-1500, 2000.

484 Tremblay, J. E., Michel, C., Hobson, K. A., Gosselin, M., and Price, N. M.: Bloom
485 dynamics in early opening waters of the Arctic Ocean. *Limnol. Oceanogr.*, 51,
486 900-912, 2006.

487 Riebesell, U., Aberle-Malzahn, N., Achterberg, E. P., Algueró-Muñiz, M.,
488 Alvarez-Fernandez, S., Arístegui, J., Bach, L. T., Boersma, M., Boxhammer, T.,
489 Guan, W. C., Haunost, M., Horn, H. G., Loscher, C. R., Ludwig, A., Spisla, C.,
490 Sswat, M., Stange, P., and Taucher, J.: Toxic algal bloom induced by ocean
491 acidification disrupts the pelagic food web, *Nat. Clim. Change*, 8, 1082-1086, 2018.

492 Wu, Y., Gao, K., and Riebesell, U.: CO₂-induced seawater acidification affects
493 physiological performance of the marine diatom *Phaeodactylum tricornutum*,

494 Biogeosciences, 7, 2915-2923, 2010.

495 Wu, Y., Campbell, D. A., Irwin, A. J., Suggett, D. J., and Finkel, Z. V.: Ocean
496 acidification enhances the growth rate of larger diatoms. *Limnol. Oceanogr.*, 59,
497 1027-1034, 2014.

498 Wulff, A., Karlberg, M., Olofsson, M., Torstensson, A., Riemann, L., Steinhoff, F. S.,
499 Mohlin, M., Ekstrand, N., and Chierici, M.: Ocean acidification and desalination:
500 Climate-driven change in a Baltic Sea summer microplanktonic community, *Mar.*
501 *Biol.*, 165, 1-15, 2018.

502 Xiao, W. P., Wang, L., Laws, E., Xie, Y. Y., Chen, J. X., Liu, X., Chen, B. Z., and Huang,
503 B. Q.: Realized niches explain spatial gradients in seasonal abundance of
504 phytoplankton groups in the South China Sea, *Prog. Oceanogr.*, 162, 223-239, 2018.

505 Xie, S., Lin, F., Zhao, X. and Gao, G.: Enhanced lipid productivity coupled with carbon
506 and nitrogen removal of the diatom *Skeletonema costatum* cultured in the high CO₂
507 level. *Algal Res.* 61, 102589, 2022.

508 Xu, J. K., Sun, J. Z., Beardall, J., and Gao, K. S.: Lower salinity leads to improved
509 physiological performance in the coccolithophorid *Emiliana huxleyi*, which partly
510 ameliorates the effects of ocean acidification, *Front. Mar. Sci.*, 7, 1-18, 2020.

511 Xu, Z. G., Gao, G., Xu, J. T., and Wu, H. Y.: Physiological response of a golden tide alga
512 (*Sargassum muticum*) to the interaction of ocean acidification and phosphorus
513 enrichment, *Biogeosciences*, 14, 671-681, 2017.

514 Yang, G. Y., and Gao, K. S.: Physiological responses of the marine diatom *Thalassiosira*
515 *pseudonana* to increased $p\text{CO}_2$ and seawater acidity, *Mar. Environ. Res.*, 79,
516 142-151, 2012.

517 Yu, P., Wang, Z. A., Churchill, J., Zheng, M., Pan, J., Bai, Y., and Liang, C.: Effects of
518 typhoons on surface seawater $p\text{CO}_2$ and air-sea CO_2 fluxes in the northern South
519 China Sea. *J. Geophys. Res-Oceans*, 125, p.e2020JC016258, 2020.

520 Yuan, X., He, L., Yin, K., Pan, G., and Harrison, P. J.: Bacterial distribution and nutrient
521 limitation in relation to different water masses in the coastal and northwestern South
522 China Sea in late summer. *Cont. Shelf Res.*, 31, 1214-1223, 2011.

523 Zhang, C., Zhang, X., Zeng, Y., Pan, W., Lin J.: Retrieval and validation of sea surface
524 temperature in the Taiwan Strait using MODIS data. *Acta Oceanol. Sin.*, 30, 153-160,
525 2008.

526 Zhang, C., Ren, Y., Cai, Y., Zeng, Y., and Zhang, X.: Study on local monitoring model for
527 SST in Taiwan strait based on MODIS data. *J. Trop. Meteorol.*, 25, 73-81, 2009.

528 Zhong, Y. P., Liu, X., Xiao, W. P., Laws, E. A., Chen, J. X., Wang, L., Liu, S. G., Zhang,
529 F., and Huang, B. Q.: Phytoplankton community patterns in the Taiwan Strait match
530 the characteristics of their realized niches, *Prog. Oceanogr.*, 186, 1-15, 2020.

531 **Figure captions**

532 **Fig. 1** Sampling stations for the incubation experiments in the Taiwan Strait and the
533 South China Sea during three cruises. Taiwan Strait cruise was conducted in July 2016
534 (red dots), South China Sea Basin cruise were conducted in September 2016 (blue dots)
535 and Western South China Sea cruise was conducted in September 2017 (black dots).

536 **Fig. 2** Temperature ($^{\circ}\text{C}$, panel a), salinity (panel b), pH_{total} (panel c), total alkalinity (μmol
537 kg^{-1} SW, panel d), and CO_2 ($\mu\text{mol kg}^{-1}$ SW, panel e) in surface seawater and mean PAR
538 intensity (W m^{-2} , panel f) during the PP incubation experiments.

539 **Fig. 3** Chl *a* concentration ($\mu\text{g L}^{-1}$) in the Taiwan Strait and the South China Sea during
540 research cruises.

541 **Fig. 4** Surface primary productivity ($\mu\text{g C } (\mu\text{g Chl } a)^{-1} \text{ d}^{-1}$) in the Taiwan Strait and the
542 South China Sea during research cruises.

543 **Fig. 5** Seawater acidification (pH decreases of 0.4 units) induced changes (%) of surface
544 primary productivity in the Taiwan Strait and the South China Sea. Red-yellow shading
545 represents a positive effect on PP and blue-purple shading represents a negative effect.

Fig. 6 Seawater acidification (pH decreases of 0.4 units) induced changes on surface primary productivity (%) in the South China Sea as a function of ambient pH_{total} (a), PAR (b), and salinity (c). The dotted lines represent 95% confidence intervals.

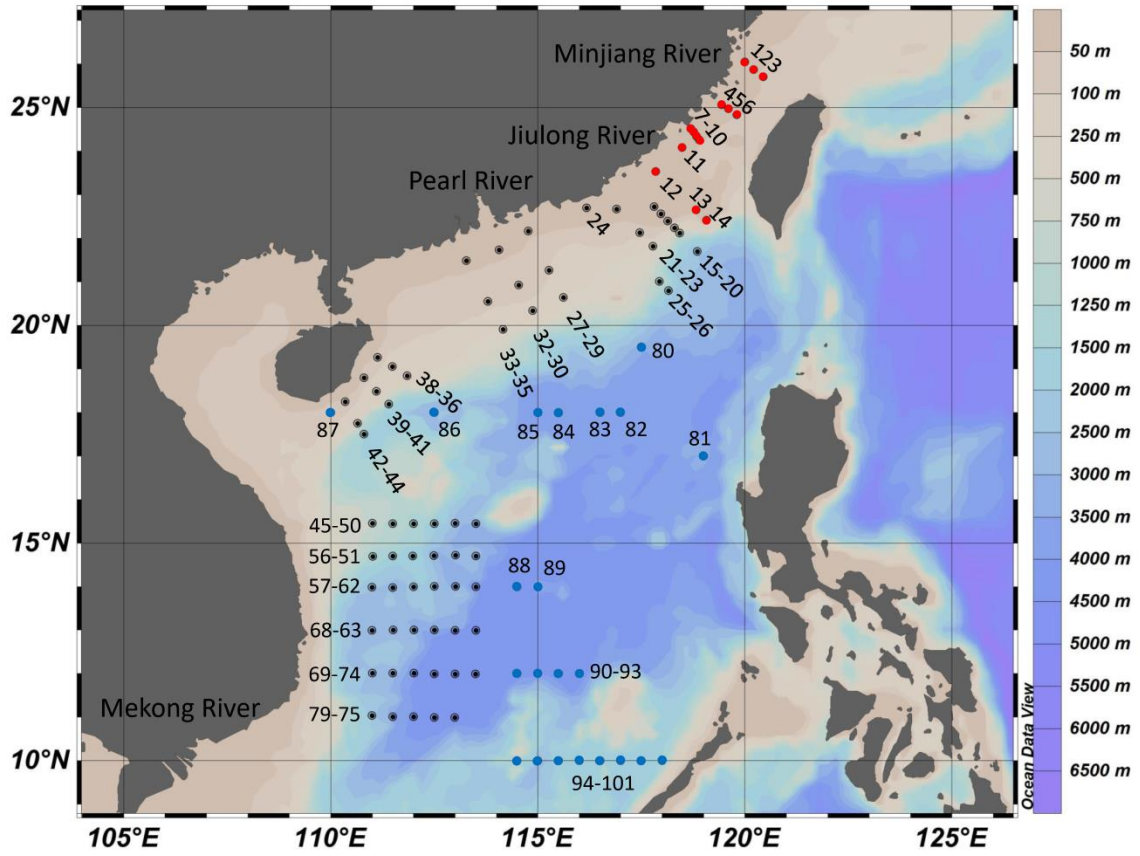


Fig. 1

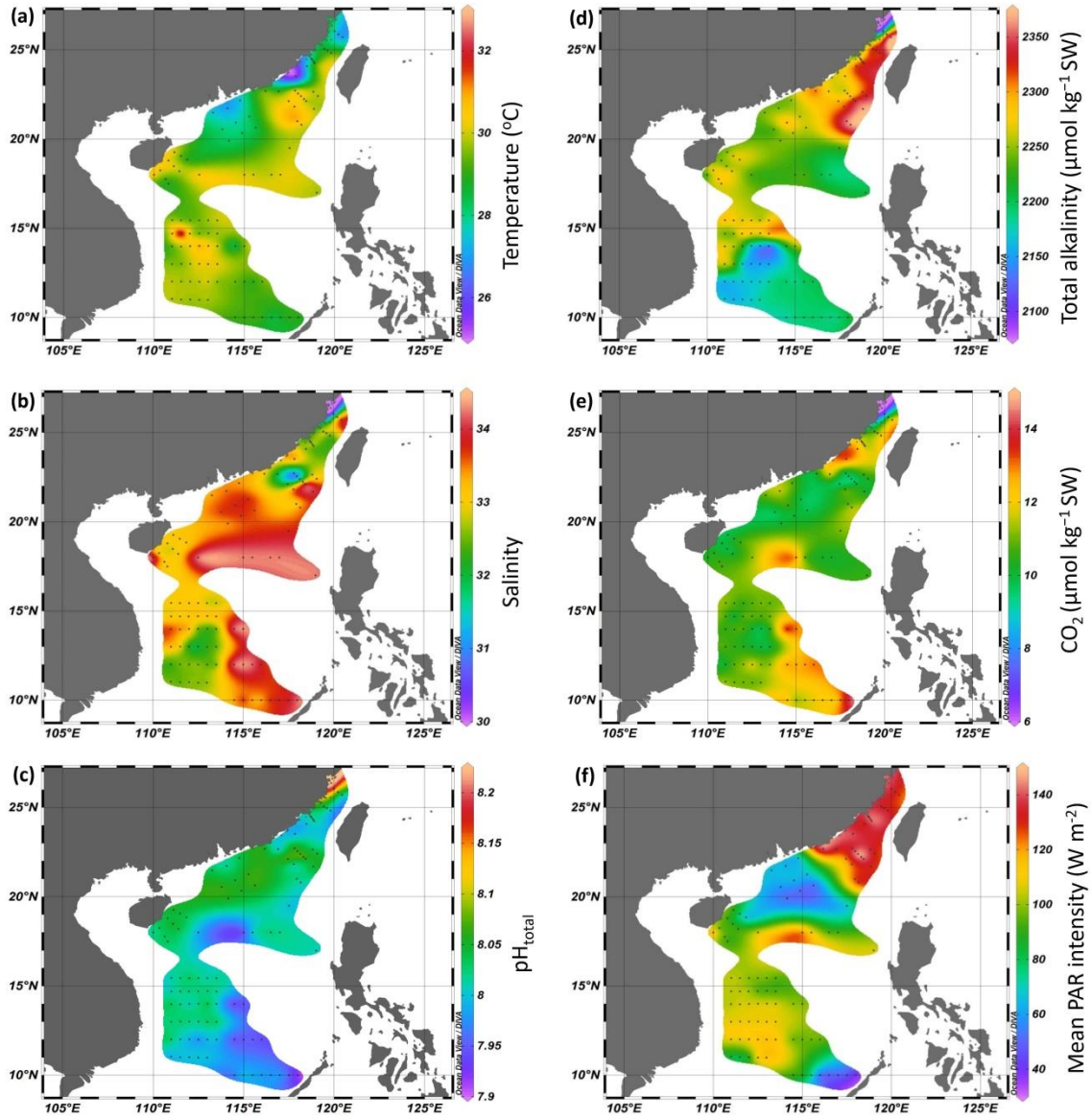


Fig. 2

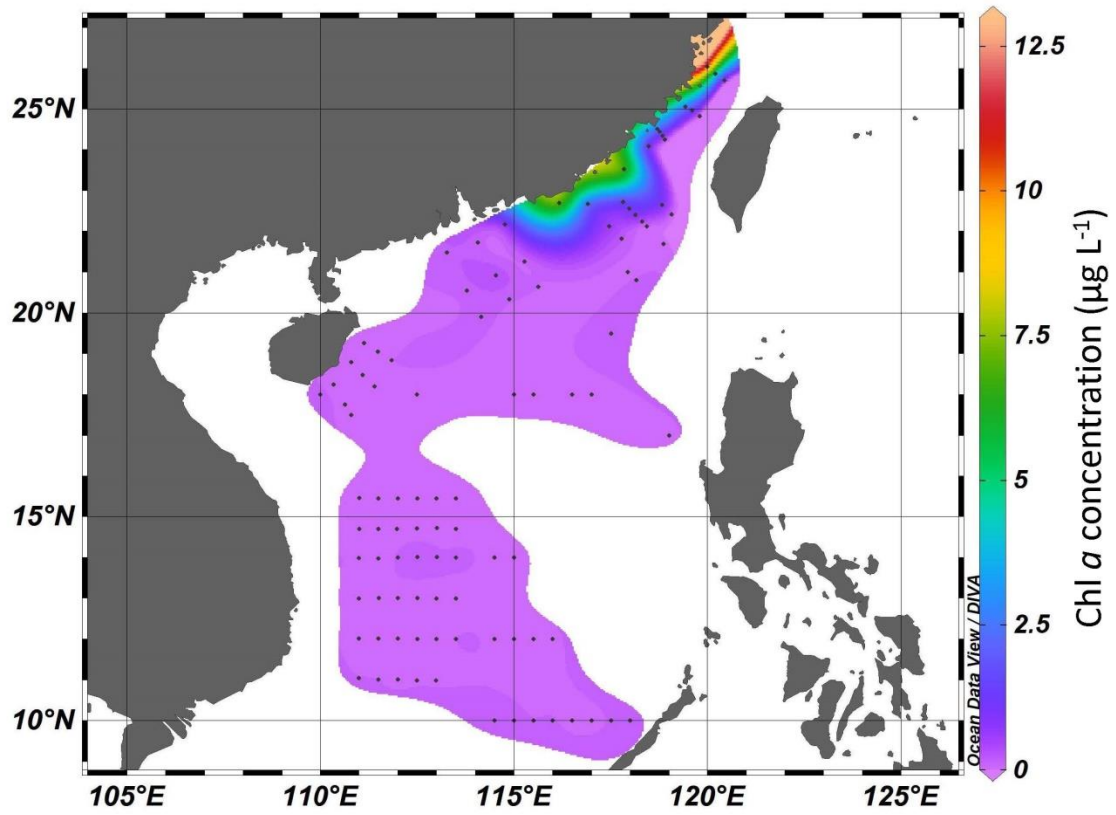


Fig. 3

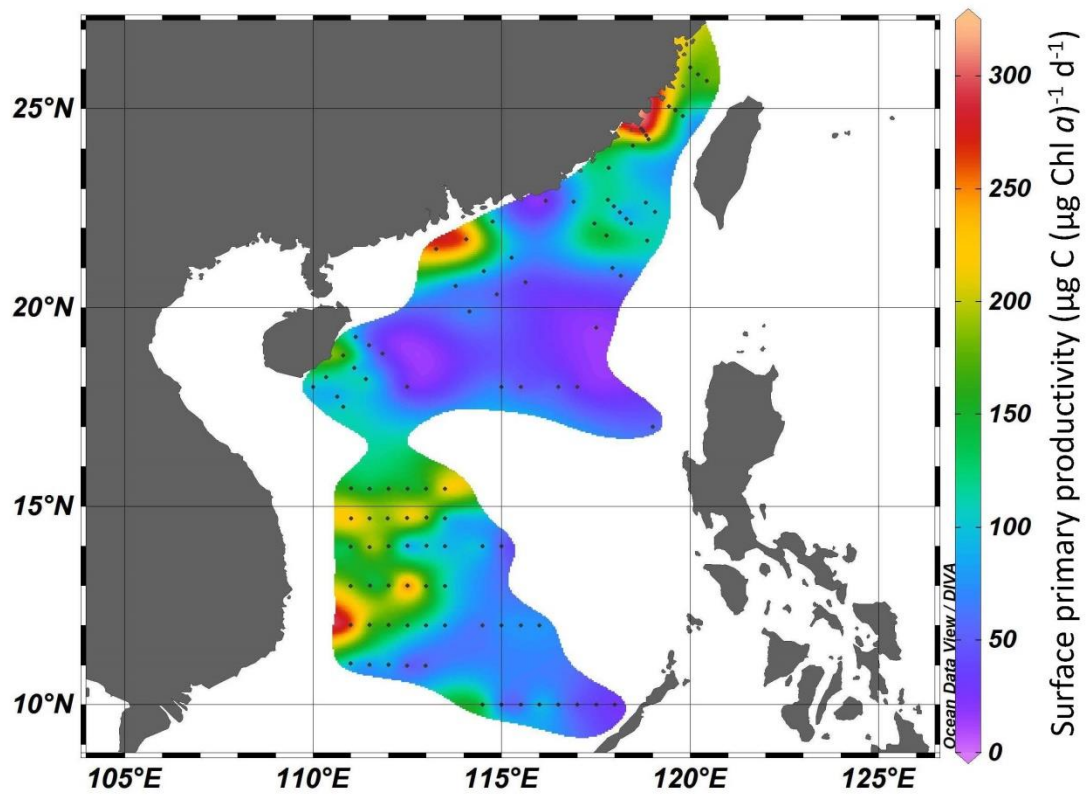


Fig. 4

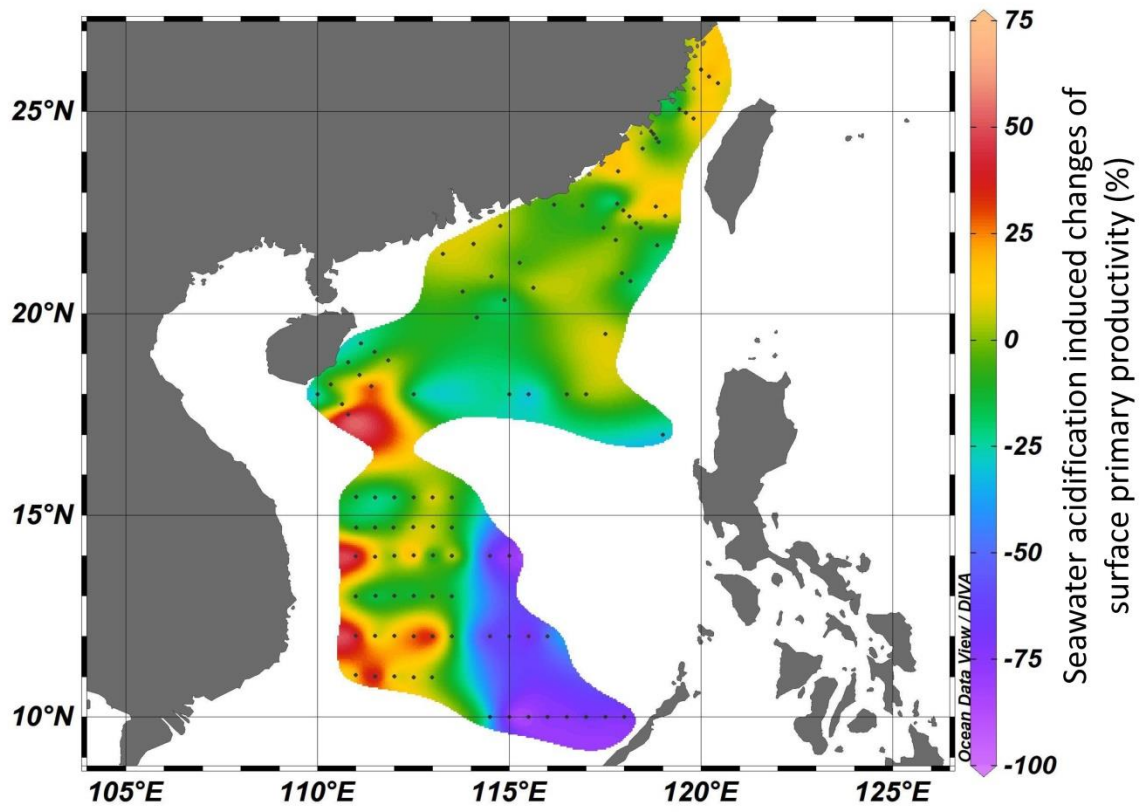


Fig. 5

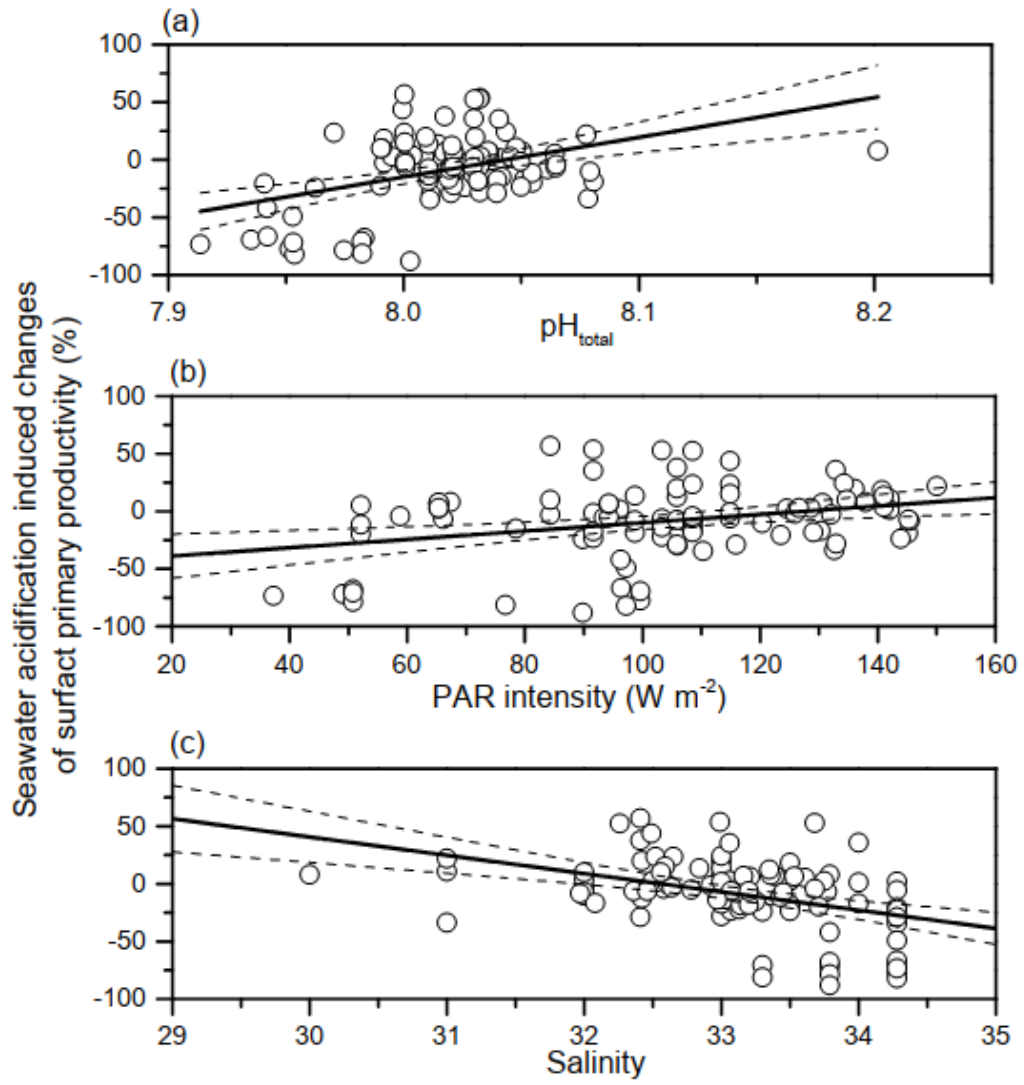


Fig. 6